PHYSICAL REVIEW B **81**, 100102(R) (2010)

Monoclinic symmetry of twin-free nanocrystals in the $BiScO_3$-$PbTiO_3$ solid solution as revealed by aberration-corrected TEM

Teresa Hungría,[1,*] Florent Houdellier,[2] Miguel Algueró,[1] and Alicia Castro[1]
[1]*Instituto de Ciencia de Materiales de Madrid (ICMM), CSIC, Cantoblanco, 28049 Madrid, Spain*
[2]*Centre d'Elaboration de Matériaux et d'Etudes Structurales (CEMES), CNRS, 29 Jeanne Marvig, 31055 Toulouse, France*
(Received 15 December 2009; revised manuscript received 8 January 2010; published 11 March 2010)

Ferroelectric perovskite solid solutions with morphotropic phase boundary (MPB) have been studied extensively as best candidates for electromechanical transduction due to their exceptionally high piezoelectric coefficients. However, despite the high number of publications about these oxides, there is still ambiguity about the actual symmetry of the phases at the MPBs. Here, we present a detailed analysis of the crystalline structure of $0.39BiScO_3$-$0.61PbTiO_3$ twin free nanocrystals, using the combination of aberration-corrected high-resolution electron microscopy and multislice simulations. Our study indicates the presence of a monoclinic symmetry for crystals with an average size of 15 nm. This is strong evidence in favor of the actual existence of this polymorph at the MPB, which has been recently questioned. It also shows that perovskite distortion is still present in nanocrystals, which is important from the point of view of the size limit of ferroelectricity and consistent with previous electrical measurements in nanostructured ceramics.

DOI: 10.1103/PhysRevB.81.100102 PACS number(s): 77.80.−e, 61.05.−a, 61.46.−w, 68.37.Og

Ferroelectric perovskite solid solutions with a morphotropic phase boundary (MPB) between ferroelectric polymorphs of rhombohedral and tetragonal symmetries present the highest known piezoelectric coefficients.[1] This is the case of $PbZr_{1-x}Ti_xO_3$ (PZT) (MPB at $x\sim0.47$, $d33\sim300$ pC N^{-1}), which is the basis of commercial, high sensitivity piezoelectric ceramics; a mature and ubiquitous technology.[2] Other examples are the relaxor-ferroelectric solid solutions $(1-x)Pb(Mg_{1/3}Nb_{2/3})O_3-xPbTiO_3$ (PMN-PT) and $(1-x)Pb(Zn_{1/3}Nb_{2/3})O_3-xPbTiO_3$ (PZN-PT), of which rhombohedral single crystals with composition close to the MPB ($x\sim0.35$ and 0.10, respectively) show ultrahigh piezoelectricity along the ⟨001⟩ direction ($d33>2000$ pC N-1).[3]

A convincing mechanism for the very high electromechanical response of these MPB materials was not proposed until 2000, after the report of a monoclinic Cm phase at the MPB of PZT.[4] This phase provided a polarization rotation path between the rhombohedral (polarization along the ⟨111⟩ direction) and tetragonal (polarization along the ⟨001⟩ direction) phases within the (110) plane. It was immediately shown theoretically and experimentally that high strain resulted from the polarization rotation under the electric field.[5,6] Recently, several works reported the existence of monoclinic phases with space groups *Pm* and *Cm* at the MPBs of the PZN-PT and PMN-PT systems.[7–10]

However, the existence of the monoclinic phases was recently questioned after the experimental observation of a significant decrease in the ferroelectric/ferroelastic domain size in PZT at the MPB down to the nanoscale[11] and of a correlation between the nanoscale domain configurations and the monoclinic distinctive features in the diffraction data.[12] It followed a demonstration by diffraction theory that nanotwin superlattices of either rhombohedral or tetragonal phases give place to effective adaptive monoclinic phases of space groups *Cm* and *Pm*, respectively, with cell parameters that are intrinsically related to those of the rhombohedral and tetragonal phases.[13,14] In this model, an effective polarization rotation can still take place under the electric field by rearrangement of the nanodomains, which has been experimentally observed.[15,16]

Nevertheless, no matter how sound and consistent these latter experimental and theoretical results are, they do not allow the conclusion that the monoclinic phases do not exist. The controversy can only be ended by studying the actual symmetry of a twin free crystal at the MPB, which is not accessible with standard methods. Indeed, only local techniques derived from the transmission electron microscopy are suitable to determine without ambiguity the symmetry of small nanodomains. This was very recently done for $PbZr_{0.54}Ti_{0.46}O_3$ in ceramics with domains of 30–100 nm width using convergent beam electron diffraction (CBED), and results indicated that the average crystal symmetry of the probed volume had to be monoclinic.[17] However, it is well known that CBED techniques cannot be used for symmetry determination in very thin crystal where dynamical effects are not sufficient to provide clear symmetry in the diffraction disks.

In our case, we have studied the crystal symmetry of twin free nanocrystals of $0.39BiScO_3$-$0.61PbTiO_3$ (composition in the MPB region of the solid solution) as small as ~10–30 nm in diameter using aberration-corrected high-resolution electron microscopy (ACHREM). We have chosen to work with nanocrystals because it is well known that twin formation is energetically unfavorable below a critical size.[18] $(1-x)BiScO_3-xPbTiO_3$ is a high Curie temperature, ferroelectric perovskite solid solution with MPB that has a lot of similarities with PZT; monoclinic *Cm* phase at the MPB, and no local cationic order or chemically inhomogeneous regions.[19–21] Coexistence of monoclinic *Cm* and tetragonal *P4mm* phases has been reported for $0.6<x<0.7$, with mainly monoclinic phase; 85%, for $x=0.61$.[20] ACHREM is an advanced microscopy technique that has allowed a step forward in qualitative and quantitative electron microscopy, providing genuine atomic resolution, so there is no doubt that it opens a range of novel possibilities in materials research.[22–25]

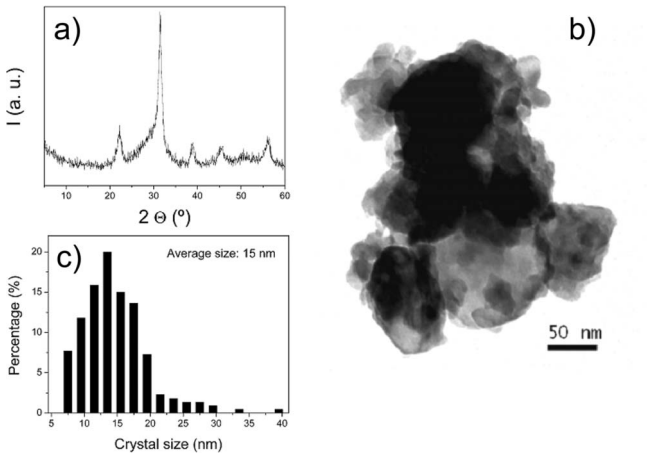

FIG. 1. (a) X-ray diffraction patterns, (b) low magnification TEM image, and (c) crystal size distribution of the $0.39BiScO_3$-$0.61PbTiO_3$ sample prepared by mechanosynthesis.

Perovskite phase $0.39BiScO_3$-$0.61PbTiO_3$ nanocrystals were obtained by mechanosynthesis from about 3 g of a stoichiometric mixture of analytical grade Bi_2O_3, Sc_2O_3, PbO, and TiO_2 (anatase). The initial mixture was placed in the stainless-steel vessel of a planetary mill (Fritsch Pulverisette 6) with five steel balls 2 cm in diameter and 35 g in weight, the grinding bowl being rotated at 300 rpm. The mechanochemical treatment was carried out in oxygen in order to avoid the Bi_2O_3 reduction, for times up to 35 h.

Crystallographic evolution during mechanical activation of the initial mixture was investigated by x-ray powder diffraction (XRD) with a Bruker AXS D8 Advance diffractometer between 5 and 60° (2θ), with 2θ increments of 0.1° and counting time of 1.5 s/step. The Cu $K\alpha$ doublet (λ=0.15418 nm) was used in these x-ray experiments. As can be observed in the XRD pattern of the final product of the mechanochemical activation process from the stoichiometric mixture [Fig. 1(a)], the $0.39BiScO_3$-$0.61PbTiO_3$ perovskite was mechanosynthesized and isolated as a single phase after the mechanical treatment. As in previous works, mechanosynthesis has shown to be a suitable preparation route to obtain nanocrystalline oxides with perovskite-type structure.[26–28] The value of the crystal size calculated from the XRD data using the Scherrer formula[29] is about 10 nm.

Crystal size obtained from the XRD was confirmed by conventional TEM (Philips CM20FEG microscope working at 200 kV), which provides reliable size distributions for such nanocrystalline powders. For all the TEM studies the powder sample was prepared in the same way: first it was crushed in an agate mortar and suspended in *n*-butanol. After ultrasonic dispersion, a droplet was deposited on a copper grid supporting a perforated carbon film. A low magnification TEM image and the Feret diameter distributions from an ensemble of more than 200 nanosized crystals for the mechanosynthesized $0.39BiScO_3$-$0.61PbTiO_3$ are shown as an example in Figs. 1(b) and 1(c), respectively.

In order to carry out the advanced structural characterization, mechanosynthesized perovskite was also investigated by ACHREM. In this case, electron microscopy observations were performed using the SACTEM Toulouse, a TECNAI

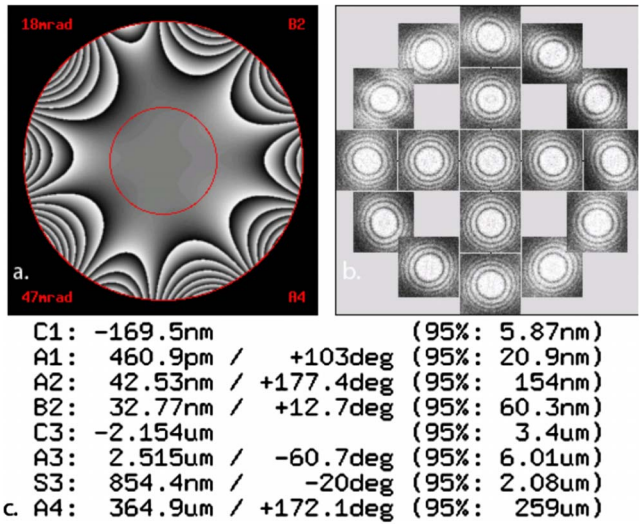

FIG. 2. (Color online) Example of a Zemlin tableau used to adjust the elements of the aberration corrector taking from a partially amorphous region close to the nanocrystal of interest.

F20 (FEI) equipped with field-emission gun (FEG) operating up to 200 kV, objective-lens spherical aberration corrector CEOS (Ref. 30) and a Gatan USC1000 2kX2k charge-coupled device camera. The microscope conditions were set and measured by the corrector software using the classical Zemlin-tableau method.[31] Aberrations are corrected up to high-order (A_1,B_2,A_2,A_3,S_3) with a C_3 value less than 1 μm. The microscope conditions have been optimized both for 200 and 100 kV. Indeed all the experiments were performed at 100 kV due to the high instability of the sample using high energy electron beam.

Conventional high-resolution transmission electron microscopy is a very efficient method for studying the structural properties of crystals at the nanoscale. However, a fine interpretation of the HREM contrast in terms of symmetry, atomic positions, etc., of the crystal requires high control of the microscope's imaging conditions. Indeed the atomic fringes contrast can be strongly affected by the phase modification of the diffracted beam coming from the uncorrected objective. To overcome these difficulties, focal series of HREM pictures are normally implemented in order to calculate and suppress numerically these phase perturbations, using dedicated software. In the case of ACHREM, we can have a perfect control of the high-order aberrations coefficients which furthermore allowed us to map the phase modification added by the system with the residual aberrations (see Fig. 2). Focal series should be implemented to suppress aberrations up to fifth-order astigmatism. Concerning our sample, we have found that these high-order aberrations have not a sufficient effect to modify the atomic contrast observed.

The use of aberration correction for imaging nanocrystalline samples has important advantages: (1) minimized delocalization of the image contrast, which results in the observation of fine details coming from high spacial frequencies components of the diffraction pattern (2) enhanced image contrast and field of view by correcting off-axial coma.[32]

As it is known, comparison between experimental fringes contrast and simulated ones for a define structure is very

TABLE I. Structural data obtained from XRD data of the mechanosynthesized $0.39BiScO_3$-$0.61PbTiO_3$ by least-squares methods.

Space group	Tetragonal *P4mm*	Rombohedral *R3m*	Monoclinic *Cm*
A (nm)	0.399	0.572	0.568
B (nm)	0.399	0.572	0.550
C (nm)	0.407	0.698	0.404
α	90	90	90
β	90	90	90.2
γ	90	120	90

problematic using conventional HREM due to the large amount of parameters which must be involved in the simulation. Thanks to the corrector, they could be easily included in the simulation. In order to retrieve the crystalline structure of the different twin free nanocrystals, multislice simulations of several ACHREM pictures of the mechanosynthesized perovskite were performed using different input structures based on literature (rhombohedral *R*3*m*, tetragonal *P*4*mm* and monoclinic *Cm*).[17,19,20] Table I summarizes the lattice parameters obtained from XRD data of the mechanosynthesized perovskite by least-squares methods by assuming these three symmetries.

Figure 2 depicts an example of the Zemlin tableau[31] used to determine the value of high-order aberrations inserted in the selected multislice simulations. The thickness has been determined assuming a spherical shape of each nanocrystal with a lateral size of 10–30 nm.

Images with a remarkable high contrast and resolution were obtained, leading to high quality fast Fourier transform (FFT) for each individual nanocrystal, even when it was necessary to set the corrector and the microscope at 100 kV acceleration voltage to avoid degradation phenomena under the beam. Through the comparison between the FFT and the simulated electron-diffraction pattern of the three possible polymorphs (tetragonal, rhombohedral, and monoclinic) it was possible to retrieve the crystallographic orientation (zone axis) of the structures under analysis. An example is shown in Fig. 3 where the detail of the HREM contrast taken on a particle of about 20 nm in size can be observed. The lower inset shows the FFT belonging to the nanosized crystal from which the zone axes of each polymorph were obtained: [001] in the case of the tetragonal *P*4*mm*, [111] for the rhombohedral *R*3*m* and [011] for the monoclinic *Cm*. As can be observed in the three upper insets belonging to the simulations of each structure in the above-mentioned orientations, the coarse structure (low spatial frequencies which contributes to the HREM contrast) fits in the three cases. However, the main advantage of using ACHREM comes from the possibility to observe the fine structure of the contrast, coming from the contribution of high spatial frequencies of the diffraction pattern. Indeed, in the aberration-free conditions, the transfer function of the microscope stays flat even for high spatial frequencies components without contrast inversion usually observed in uncorrected microscope.[33] Then, all the spatial frequencies are equally transmitted by the optical system without any delocalization. As a result, due to the contribution of these diffracted beams, very small interference fringes, directly related to the object fine atomic structure, induced fine details as, for example, can be observed in Fig. 3 where secondary spots appeared in the middle ground of the image, which can then be directly compared with simulated contrast performed by the multislice algorithm using the chosen structure and the microscope conditions given by the corrector. In the case of the nanocrystal shown in Fig. 3, it is possible to see that only in the case of the monoclinic symmetry the fine structure of the simulation fits perfectly. Furthermore, at 100 keV with a phase plate change less than $\pi/4$ on a tilt range of 20 mrad, it is possible to have access to aberration-free fine fringes of 0.185 nm. This value is sufficiently important to assess the reliability of the symmetry comparison results regarding small variations of the microscope conditions. In order to be sure, systematic simulations have been carried out, and the symmetry is not affected by the artifacts such as illumination tilt which add off-axial coma and thickness in a range of $+/-10$ nm, what is large enough in this kind of nanocrystalline samples.

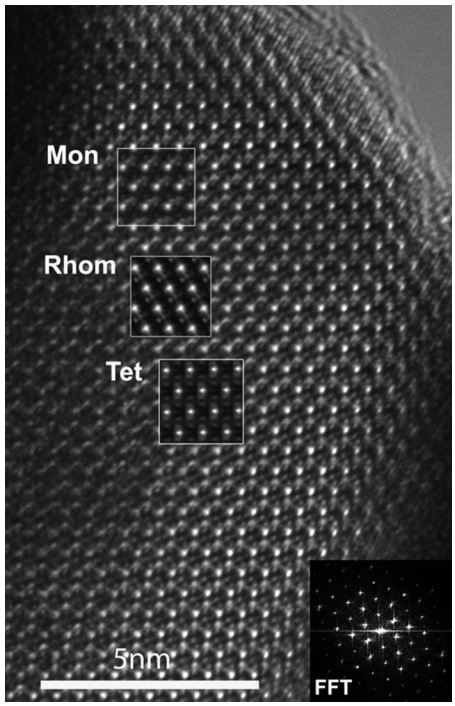

FIG. 3. HREM image of a crystal of 20 nm of the $0.39BiScO_3$-$0.61PbTiO_3$ sample. Lower inset: FFT of the nanosized crystal. Upper insets: simulation of the three polymorphs in different zone axis (Tet=tetragonal symmetry, zone axes [001]; Rhom =rhombohedra symmetry, zone axes [111]; and Mon=monoclinic symmetry, zone axes [011]).

This nanocrystal is not an isolated case, and it is possible to find numerous examples with sizes between 10 and 30 nm with monoclinic symmetry and randomly oriented. Figure 4 depicts the HREM micrograph of a 15 nm crystal together with the simulation of the Cm polymorph with [100] orientation. It was also possible to identify some particles with tetragonal symmetry; however the great majority of the cases present the monoclinic one what is in good agreement with

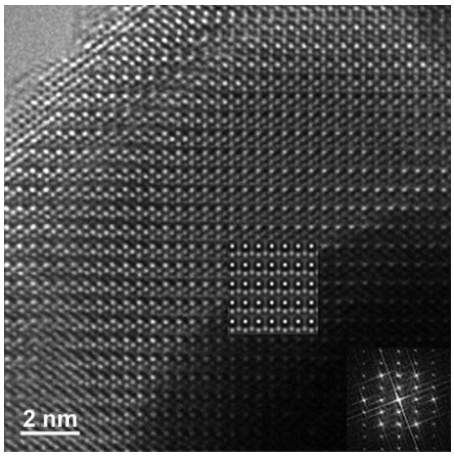

FIG. 4. HREM image of a crystal of 15 nm of the $0.39BiScO_3$-$0.61PbTiO_3$ perovskite. Lower inset: FFT of the nanosized crystal. Upper inset: Simulation of the monoclinic polymorph with the [100] orientation.

that obtained by Rietveld analysis of XRD data.[20] Therefore, these results clearly revealed the monoclinic symmetry of twin free nanocrystals in the $BiScO_3$-$PbTiO_3$ solid solution, and they are a strong evidence that monoclinic phases at MPBs are not the result of the nanotwin superlattices of the other polymorphs.

Results here reported are also relevant to another highly topical issue: the size limit for ferroelectricity. This is a cooperative phenomenon, and thus the existence of a fundamental size limit below which ferroelectricity vanishes is expected.[34] As far as perovskite nanoparticles are concerned, tetragonal distortion has been found to persist in $BaTiO_3$ and $PbTiO_3$ nanoparticles as small as 26 and 20 nm, respectively.[35,36] This parameter is directly associated with the spontaneous polarization, which was indirectly measured for $PbTiO_3$ particles of 28 nm.[37] Also, local ferroelectricity has been demonstrated in $BaTiO_3$ nanoparticles of 25 nm.[38] In relation to MPB perovskites, predominant tetragonal phase has been reported for PZT nanoparticles of 30 nm by Rietveld analysis of XRD data.[39] Unlike in PZT, ferroelectric order does not develop in nanoscale relaxor based materials, and instead the high-temperature relaxor state is stabilized.[40,41] In this work and in the case of MPB $BiScO_3$-$PbTiO_3$, monoclinic symmetry is found for nanocrystals as small as 10 nm.

In summary, our study indicates the existence of the monoclinic polymorph in the MPB region of the $BiScO_3$-$PbTiO_3$ solid solution, which has been revealed in crystals with size between 10 and 30 nm. This is strong evidence in favor of the actual existence of this phase in MPBs between rhombohedral and tetragonal phases of ferroelectric perovskite solid solutions, a controversial issue within the ferroelectric materials field. This result also indicate that the polar phase persist in the nanoscale, which is in good agreement with our recent results where ferroelectric switching was clearly demonstrated for nanostructured ceramics of this system prepared by spark plasma sintering.[42] These results compare favorably with those reported for relaxor based MPB systems, for which the high-temperature relaxor state was stabilized at room temperature as a size effect, and no ferroelectric long-range order develops.

This work has been funded by MEC (Spain) through the Projects No. MAT2007-61884 and No. MAT2008-02003/NAN. T.H. is indebted to the CSIC (MICINN) of Spain for the "Junta de Ampliación de Estudios" contract (Reference No. JAEDOC082). Technical support by I. Martínez (ICMM) is also acknowledged.

*Corresponding author. FAX: +34 913720623; thungria@icmm.csic.es

[1] W. Cao and L. E. Cross, Phys. Rev. B **47**, 4825 (1993).
[2] N. Setter, *Piezoelectric Materials in Devices* (EPFL, Lausanne, 2002).
[3] S. E. Park and T. R. Shrout, J. Appl. Phys. **82**, 1804 (1997).
[4] B. Noheda *et al.*, Phys. Rev. B **61**, 8687 (2000).
[5] H. Fu and R. E. Cohen, Nature (London) **403**, 281 (2000).
[6] R. Guo *et al.*, Phys. Rev. Lett. **84**, 5423 (2000).
[7] B. Noheda *et al.*, Phys. Rev. Lett. **86**, 3891 (2001).
[8] J. M. Kiat *et al.*, Phys. Rev. B **65**, 064106 (2002).
[9] B. Noheda *et al.*, Phys. Rev. B **66**, 054104 (2002).
[10] A. K. Singh and D. Pandey, Phys. Rev. B **67**, 064102 (2003).
[11] L. A. Schmitt *et al.*, J. Appl. Phys. **101**, 074107 (2007).
[12] K. A. Schonau *et al.*, Phys. Rev. B **75**, 184117 (2007).
[13] Y. U. Wang, Phys. Rev. B **74**, 104109 (2006).
[14] Y. U. Wang, Phys. Rev. B **76**, 024108 (2007).
[15] Y. M. Jin *et al.*, Phys. Rev. Lett. **91**, 197601 (2003).
[16] K. A. Schonau *et al.*, Phys. Rev. B **76**, 144112 (2007).
[17] R. Schierholz *et al.*, Phys. Rev. B **78**, 024118 (2008).
[18] G. Arlt, J. Mater. Sci. **25**, 2655 (1990).
[19] R. E. Eitel *et al.*, J. Appl. Phys. **96**, 2828 (2004).
[20] J. Chaigneau *et al.*, Phys. Rev. B **76**, 094111 (2007).
[21] B. Kim *et al.*, J. Appl. Phys. **105**, 114101 (2009).
[22] K. W. Urban, Nature Mater. **8**, 260 (2009).
[23] K. W. Urban, Science **321**, 506 (2008).
[24] M. Hÿtch *et al.*, Nature (London) **453**, 1086 (2008).
[25] C. L. Johnson *et al.*, Nature Mater. **7**, 120 (2008).
[26] T. Hungría *et al.*, Chem. Mater. **17**, 6205 (2005).
[27] M. Algueró *et al.*, Chem. Mater. **19**, 4982 (2007).
[28] T. Hungría *et al.*, Nanotechnology **19**, 155609 (2008).
[29] B. D. Cullity, *Elements of X-ray Diffraction; Series in Metallurgy and Materials* (Addison-Wesley, Reading, MA, 1967).
[30] H. Rose, Optik (Stuttgart) **85**, 19 (1990).
[31] F. Zemlin *et al.*, Ultramicroscopy **3**, 49 (1978).
[32] F. Houdellier *et al.*, *Advances in Imaging and Electron Physics* (Elsevier Inc., San Diego, CA, 2008), Vol. 153, Chap. 6.
[33] J. C. H. Spence, *Experimental High-Resolution Electron Microscopy* (Oxford University Press, New York, 1980).
[34] N. A. Spaldin, Science **304**, 1606 (2004).
[35] S. Chattopadhyay *et al.*, Phys. Rev. B **52**, 13177 (1995).
[36] M. B. Smith *et al.*, J. Am. Chem. Soc. **130**, 6955 (2008).
[37] E. K. Akdogan *et al.*, J. Appl. Phys. **97**, 084305 (2005).
[38] S. Ray *et al.*, Small **2**, 1427 (2006).
[39] C. Liu *et al.*, J. Am. Chem. Soc. **123**, 4344 (2001).
[40] J. Carreaud *et al.*, Phys. Rev. B **72**, 174115 (2005).
[41] M. Algueró *et al.*, Small **3**, 1906 (2007).
[42] M. Algueró *et al.*, Appl. Phys. Lett. **94**, 012902 (2009).